NICST Internal Memo

Date: May 25, 2010
From: J. McIntire
To: Bruce Guenther, Jim Butler, and Jack Xiong
Subject: VIIRS F1 RC-01 Part 4 RSB Gain Transition Analysis

References:

[1] 'Radiometric Characterization RC-1 – VIIRS,' TP154640-270_B.
[2] 'Sensor Performance Verification Plan (PVP) - VIIRS,' PVP154640-101_RevA-5.
[3] NICST_REPORT_09_043, 'Analysis of VIIRS FU1 GTA from T-VAC RC-01 P4 Cold Performance,' C. Pan, A. Liu, and J. McIntire, June 17, 2009.
[4] 'Performance Specification Sensor Specification,' ps154640-101_c.
[5] W043,'Request to Modify Dual Gain Transition requirement (SRV0465) in the VIIRS Sensor Specification,' January 15, 2007.
[6] ST_RSB_radiometric_final, 'VIIRS F1 Pre-launch calibration and Characterization: Reflective Solar Band Radiometry,' January 25, 2010.
[7] NICST_MEMO_10_010, 'Summary of F1 radiometric calibration Performance for RSB from RC-02 TV tests,' J. Sun and N. Che, May 3, 2010.
[8] NICST_REPORT_10_008, 'Preliminary Investigation of SIS100 Red Leak,' J. McIntire, A. Tolea, N. Che, April 27, 2010.

1. Introduction

The assessment of dual gain band transition was performed during TV testing as RC-01 Part 4 at Cold plateau [1,2]. This work will focus on the RSB gain switching (bands M1-M5 and M7). The test data used here is listed in Table 1 (where only data utilizing the SIS100 source is included). The SIS100 levels listed refer to the number of lamps on (8W-45W-200W). Preliminary findings were reported in [3].

SRV0465 states that the gain transition shall occur at a scene radiance between L_{MAX} and $1.5L_{MAX}$ for M1 and M2 and between L_{MAX} and $1.2L_{MAX}$ for M3, M4, M5, and M7 [4]. In addition, the wavier W043 has requested that the upper bound in the specification for all dual gain RSB bands be relaxed to $1.5L_{MAX}$ [5]. This work will assess this specification for electronics side A only (B side was not measured during RC-01 Part 4).

2. Data Analysis

This section describes the data processing. First, the SV DN is averaged over samples. Then, this sample averaged SV DN is subtracted from each sample of the EV DN. The EV sample range selected for this work was 0 – 799; this range encompasses the SIS100 view entirely (as seen in Figure 1).

The gain switching is evaluated at both the initial switch point (high gain to low gain transition) as well as the final switch point (low gain to high gain switch point). The high to low switch dn is defined as the maximum high gain dn between the minimum sample (0) and the first sample in low gain; similarly, the low to high switch dn is determined by locating the maximum high gain dn between the last low gain sample and the maximum sample (799). This calculation is performed for all scans and then scan averaged. The maximum dn at transition over collects is then determined.

The specified L_{MAX} is converted into dn [2] using the coefficients determined from RC-02 Parts 1 and 3 [6-7]. Then, these switch dn are evaluated against the specification SRV0465 [4] in dn space.

3. SIS100 Red Leak Correction

The SIS100 is known to be "redder" than the solar irradiance profile. As a result, for bluer bands Out Of Band (OOB) filter leaks contribute to the radiance reaching the detector (particularly for M1). In consequence, the gains for these bands are under-reported. The gain transition itself is a property of the electronics, and as such is not directly affected by the red leak. However, in order to compare the dn at the gain transition to the specification, L_{MAX} must be converted to dn (or the dn at transition must be converted to radiance). This influences the compliance of the gain transition for M1. Preliminary investigation of this "red leak' was conducted [8] and the correction factors developed there are applied to this analysis.

4. Analysis Results

The gain transition results for M1 are shown in Table 2. The high gain dn at the gain transition point is listed for each detector and HAM side as well as for both high to low and low to high transitions. For M1, the dn at transition is roughly 3350 – 3400, which is about 82 – 83 % of 4095 (ADC saturation) and between 125 – 132 % of dn at L_{MAX}. Results from the high to low and low to high transitions are comparable. The radiance at the transition for each detector (HAM side A) for both the low to high and high to low transitions are plotted in Figure 2. The red dashed lines are the specified limits on the gain transition. The transition point is well within the specified limits for all detectors. Figure 3 shows the dn, standard deviation, and SNR at each sample in the selected range for band M1 detector 9, HAM side A (collect 3). The high gain samples are in red and the low gain samples are in blue. There is a little noise evident in the SNR plot near the transition, but on the whole the gain transition behaved as expected. This noise is the manifestation of the dual gain anomaly; analysis of this anomaly is the subject of future work.

Note that if the SIS100 red leak correction had not been applied to the M1 gain, the dn at transition was between 90 – 95 % of dn at L_{MAX}, which is below the specified lower limit. In [7], pre-saturation was observed for M1. However, using the SIS100 red leak

correction to determine the true saturation radiance for M1 indicates that no pre-saturation occurs (in fact, saturation occurs above the gain transition point).

Table 3 lists the gain transition results for M2. Both the high to low and low to high transitions occur at roughly 3350 – 3400 dn, which is about 82 – 83 % of 4095 (ADC saturation). In the case of M2, this transition takes place at approximately 108 – 113 % of the response at L_{MAX}. This is comfortably within the specified limits (as seen in Figure 4). Figure 5 graphs the dn, standard deviation, and SNR at each sample in the selected range for data from collect 3 and band M2 detector 9, HAM side A. Again, there appears to be some small noise near the transition. However, this does not appear to affect the gain switching performance.

The results of the gain transition for M3 are shown in Table 4. The high to low and low to high transitions both occur at around 3400 – 3450 dn. This corresponds to roughly 83 – 84 % of ADC saturation (4095). In terms of compliance with the specification, the dn at transition is approximately 116 – 119 % of the response at L_{MAX} (this is within the allowed tolerance of $1.2L_{MAX}$). Figure 6 shows the detector dependence of the radiance at transition and compares it to the specified limits. Figure 7 plots the dn, standard deviation, and SNR at each sample for band M3, detector 9 and HAM side A from collect 11. The M3 gain transition behaves as expected.

The M4 high to low and low to high transitions both occur in the range 3385 – 3430 dn, which is about 83 – 84 % of ADC saturation (4095). These results are shown in Table 4. The transitions occur at approximately 112 – 115 % of L_{MAX}; this is within the specified limits for M4. The compliance of each individual detector is shown in Figure 8. The dn, standard deviation, and SNR for M4 detector 9, HAM side A from collect 11 are shown in Figure 9. There is some small noise near the transition, but the transition occurs as expected.

The gain transition results for band M5 are shown in Table 5. The dn at transition for both high to low and low to high transitions is around 3370 – 3415 dn. This corresponds to 82 – 84 % of 4095 (ADC saturation). The transition occurs between 111 and 113 % of L_{MAX}, which is below the upper limit of $1.2L_{MAX}$. Figure 10 shows the gain transition radiance for each detector in comparison to the specified limits. Figure 11 plots the dn, standard deviation, and SNR for M5 detector 9, HAM side A from collect 13. There is some small variation in SNR near the transition, but M5 transitions as expected.

Table 6 lists the gain transition results for band M7. The high to low and low to high transitions occur around 3400 – 3460 dn (or about 83 – 84 % of ADC saturation). The transition occurs between 106 and 108 % of L_{MAX} (the bounds are L_{MAX} and $1.2L_{MAX}$). The detector by detector compliance with the specification is shown in Figure 12. Figure 13 plots the dn, standard deviation, and SNR for each sample in the selected range for M7 detector 9, HAM A for collect 13. Some small noise is evident near the switch point, but the gain transition behaves as expected.

5. Summary

- The gain transition for the all of RSB bands (M1 – M5 and M7) was within the specified bounds set by SRV0465 ($L_{MAX} - 1.5L_{MAX}$ for M1 – M2 and $L_{MAX} - 1.2l_{MAX}$ for M3 – M5 and M7).
- Using the SIS100 red leak correction is necessary to determine the true gain transition radiance for M1. Furthermore, this correction also indicates that no pre-saturation occurs for M1. As a result, the RSB gain transitions behave as expected.

Acknowledgement

The sensor test data used in this document was provided by the Raytheon El Segundo testing team. Approaches for data acquisition and data reductions, as well as data extraction tools were also provided by the Raytheon El Segundo team. We would like to thank the Raytheon El Segundo team for their support. The data analysis tools were developed by the NICST team, and we would like to extend our gratitude for their valued assistance.

Table 1: VIIRS FU1 RC-01 Part 4 gain transition data

Test	Part	Plateau	UAID	E side	Collect	Vref gain	SIS100 Level
RC-01	4	Cold	U3103353	A	1	-3.572	10--9--18
RC-01	4	Cold	U3103353	A	2	-3.574	10--9--18
RC-01	4	Cold	U3103353	A	3	-3.584	10--9--18
RC-01	4	Cold	U3103353	A	4	-3.551	10--9--18
RC-01	4	Cold	U3103353	A	5	-3.538	10--9--18
RC-01	4	Cold	U3103353	A	6	-3.531	10--9--18
RC-01	4	Cold	U3103353	A	7	-3.572	10--9--18
RC-01	4	Cold	U3103353	A	8	-3.570	10--9--18
RC-01	4	Cold	U3103353	A	9	-3.570	10--9--18
RC-01	4	Cold	U3103353	A	10	-3.570	10--9--10
RC-01	4	Cold	U3103353	A	11	-3.570	10--9--3
RC-01	4	Cold	U3103353	A	12	-3.570	10--9--0
RC-01	4	Cold	U3103353	A	13	-3.570	10--3--0
RC-01	4	Cold	U3103353	A	14	-3.570	10--1--0

Table 2: M1 gain transition from RC-01 Part 4 Cold plateau

Band	HAM	Detector	High to Low Transition			Low to High Transition		
			dn at transistion	% of 4095	% of dn_{MAX}	dn at transistion	% of 4095	% of dn_{MAX}
M1	A	1	3400.6	83.0%	132.8%	3401.8	83.1%	132.8%
M1	A	2	3384.6	82.7%	129.0%	3383.4	82.6%	129.0%
M1	A	3	3378.3	82.5%	127.7%	3377.4	82.5%	127.7%
M1	A	4	3381.3	82.6%	127.2%	3377.3	82.5%	127.0%
M1	A	5	3369.8	82.3%	125.3%	3369.5	82.3%	125.3%
M1	A	6	3387.6	82.7%	126.7%	3384.6	82.7%	126.6%
M1	A	7	3410.9	83.3%	129.3%	3410.4	83.3%	129.3%
M1	A	8	3365.1	82.2%	126.9%	3369.8	82.3%	127.1%
M1	A	9	3376.7	82.5%	126.3%	3382.1	82.6%	126.5%
M1	A	10	3390.0	82.8%	126.8%	3384.1	82.6%	126.6%
M1	A	11	3378.1	82.5%	126.7%	3383.0	82.6%	126.9%
M1	A	12	3376.8	82.5%	125.9%	3381.9	82.6%	126.1%
M1	A	13	3391.3	82.8%	126.1%	3391.4	82.8%	126.1%
M1	A	14	3396.6	82.9%	129.8%	3391.3	82.8%	129.6%
M1	A	15	3372.1	82.3%	128.9%	3364.0	82.1%	128.6%
M1	A	16	3378.0	82.5%	129.8%	3371.9	82.3%	129.6%
M1	B	1	3402.2	83.1%	132.8%	3399.5	83.0%	132.7%
M1	B	2	3383.7	82.6%	129.0%	3382.0	82.6%	128.9%
M1	B	3	3382.7	82.6%	127.9%	3374.8	82.4%	127.6%
M1	B	4	3375.5	82.4%	126.9%	3378.6	82.5%	127.0%
M1	B	5	3367.4	82.2%	125.2%	3368.0	82.2%	125.3%
M1	B	6	3384.1	82.6%	126.6%	3384.6	82.7%	126.6%
M1	B	7	3407.6	83.2%	129.2%	3406.6	83.2%	129.2%
M1	B	8	3367.6	82.2%	127.0%	3369.7	82.3%	127.1%
M1	B	9	3380.5	82.6%	126.4%	3381.8	82.6%	126.5%
M1	B	10	3381.9	82.6%	126.5%	3382.4	82.6%	126.5%
M1	B	11	3375.4	82.4%	126.6%	3385.4	82.7%	127.0%
M1	B	12	3381.0	82.6%	126.1%	3382.2	82.6%	126.1%
M1	B	13	3393.8	82.9%	126.2%	3391.4	82.8%	126.1%
M1	B	14	3390.9	82.8%	129.6%	3390.0	82.8%	129.6%
M1	B	15	3370.8	82.3%	128.8%	3362.9	82.1%	128.5%
M1	B	16	3372.1	82.3%	129.6%	3368.6	82.3%	129.4%

Table 3: M2 gain transition from RC-01 Part 4 Cold plateau

Band	HAM	Detector	High to Low Transition			Low to High Transition		
			dn at transistion	% of 4095	% of dn_{MAX}	dn at transistion	% of 4095	% of dn_{MAX}
M2	A	1	3385.9	82.7%	110.4%	3377.8	82.5%	110.1%
M2	A	2	3387.6	82.7%	109.9%	3382.6	82.6%	109.7%
M2	A	3	3364.1	82.2%	109.4%	3374.8	82.4%	109.7%
M2	A	4	3383.2	82.6%	109.5%	3384.5	82.7%	109.5%
M2	A	5	3358.8	82.0%	108.2%	3361.8	82.1%	108.3%
M2	A	6	3389.6	82.8%	109.7%	3386.4	82.7%	109.6%
M2	A	7	3383.1	82.6%	109.5%	3363.3	82.1%	108.8%
M2	A	8	3390.8	82.8%	109.7%	3365.1	82.2%	108.9%
M2	A	9	3376.7	82.5%	109.3%	3372.9	82.4%	109.2%
M2	A	10	3404.3	83.1%	110.4%	3392.0	82.8%	110.0%
M2	A	11	3402.8	83.1%	110.4%	3381.9	82.6%	109.7%
M2	A	12	3378.1	82.5%	109.6%	3377.4	82.5%	109.6%
M2	A	13	3403.9	83.1%	110.7%	3399.0	83.0%	110.5%
M2	A	14	3382.5	82.6%	111.0%	3378.4	82.5%	110.9%
M2	A	15	3383.6	82.6%	112.6%	3397.6	83.0%	113.1%
M2	A	16	3374.3	82.4%	112.6%	3385.3	82.7%	113.0%
M2	B	1	3398.5	83.0%	110.8%	3382.9	82.6%	110.3%
M2	B	2	3373.7	82.4%	109.4%	3389.0	82.8%	109.9%
M2	B	3	3378.1	82.5%	109.8%	3380.6	82.6%	109.9%
M2	B	4	3376.8	82.5%	109.3%	3373.9	82.4%	109.2%
M2	B	5	3370.8	82.3%	108.6%	3354.9	81.9%	108.1%
M2	B	6	3402.4	83.1%	110.1%	3378.2	82.5%	109.3%
M2	B	7	3369.1	82.3%	109.0%	3367.1	82.2%	109.0%
M2	B	8	3378.7	82.5%	109.3%	3368.5	82.3%	109.0%
M2	B	9	3382.3	82.6%	109.5%	3368.0	82.2%	109.0%
M2	B	10	3381.7	82.6%	109.7%	3398.6	83.0%	110.3%
M2	B	11	3379.8	82.5%	109.6%	3385.6	82.7%	109.8%
M2	B	12	3383.0	82.6%	109.7%	3376.5	82.5%	109.5%
M2	B	13	3376.6	82.5%	109.8%	3383.2	82.6%	110.0%
M2	B	14	3396.9	83.0%	111.5%	3376.3	82.4%	110.8%
M2	B	15	3395.7	82.9%	113.1%	3376.7	82.5%	112.4%
M2	B	16	3387.4	82.7%	113.0%	3387.6	82.7%	113.0%

Table 4: M3 gain transition from RC-01 Part 4 Cold plateau

Band	HAM	Detector	High to Low Transition			Low to High Transition		
			dn at transistion	% of 4095	% of dn_{MAX}	dn at transistion	% of 4095	% of dn_{MAX}
M3	A	1	3429.5	83.7%	118.6%	3425.1	83.6%	118.5%
M3	A	2	3429.4	83.7%	118.6%	3411.4	83.3%	118.0%
M3	A	3	3429.4	83.7%	117.7%	3427.6	83.7%	117.6%
M3	A	4	3421.4	83.5%	117.4%	3415.6	83.4%	117.2%
M3	A	5	3420.7	83.5%	116.7%	3410.8	83.3%	116.4%
M3	A	6	3414.1	83.4%	115.9%	3416.0	83.4%	115.9%
M3	A	7	3437.5	83.9%	117.3%	3425.3	83.6%	116.9%
M3	A	8	3442.5	84.1%	117.5%	3420.7	83.5%	116.7%
M3	A	9	3439.2	84.0%	117.0%	3448.5	84.2%	117.3%
M3	A	10	3442.2	84.1%	117.5%	3436.5	83.9%	117.3%
M3	A	11	3422.6	83.6%	117.1%	3423.8	83.6%	117.1%
M3	A	12	3458.3	84.5%	119.0%	3440.0	84.0%	118.3%
M3	A	13	3420.1	83.5%	116.7%	3418.9	83.5%	116.7%
M3	A	14	3434.0	83.9%	118.1%	3448.5	84.2%	118.6%
M3	A	15	3434.7	83.9%	118.8%	3434.0	83.9%	118.8%
M3	A	16	3431.1	83.8%	119.0%	3425.1	83.6%	118.8%
M3	B	1	3433.5	83.8%	118.8%	3425.9	83.7%	118.5%
M3	B	2	3410.6	83.3%	118.0%	3409.9	83.3%	117.9%
M3	B	3	3431.0	83.8%	117.7%	3425.9	83.7%	117.5%
M3	B	4	3419.9	83.5%	117.3%	3422.6	83.6%	117.4%
M3	B	5	3410.0	83.3%	116.4%	3406.3	83.2%	116.2%
M3	B	6	3412.7	83.3%	115.8%	3412.1	83.3%	115.8%
M3	B	7	3426.6	83.7%	116.9%	3426.5	83.7%	116.9%
M3	B	8	3424.3	83.6%	116.8%	3419.9	83.5%	116.7%
M3	B	9	3439.1	84.0%	117.0%	3447.3	84.2%	117.3%
M3	B	10	3441.6	84.0%	117.4%	3439.6	84.0%	117.4%
M3	B	11	3423.6	83.6%	117.1%	3423.0	83.6%	117.1%
M3	B	12	3441.1	84.0%	118.4%	3442.5	84.1%	118.4%
M3	B	13	3421.0	83.5%	116.7%	3415.7	83.4%	116.5%
M3	B	14	3433.8	83.9%	118.1%	3436.5	83.9%	118.2%
M3	B	15	3434.8	83.9%	118.8%	3431.4	83.8%	118.7%
M3	B	16	3428.8	83.7%	118.9%	3424.9	83.6%	118.8%

Table 5: M4 gain transition from RC-01 Part 4 Cold plateau

Band	HAM	Detector	High to Low Transition			Low to High Transition		
			dn at transistion	% of 4095	% of dn_{MAX}	dn at transistion	% of 4095	% of dn_{MAX}
M4	A	1	3403.0	83.1%	115.0%	3402.5	83.1%	115.0%
M4	A	2	3430.7	83.8%	115.5%	3416.1	83.4%	115.0%
M4	A	3	3396.9	83.0%	113.5%	3394.5	82.9%	113.4%
M4	A	4	3404.4	83.1%	113.8%	3401.4	83.1%	113.7%
M4	A	5	3410.8	83.3%	113.6%	3410.8	83.3%	113.6%
M4	A	6	3397.2	83.0%	112.7%	3393.7	82.9%	112.6%
M4	A	7	3415.5	83.4%	112.9%	3406.0	83.2%	112.6%
M4	A	8	3413.3	83.4%	112.8%	3396.7	82.9%	112.2%
M4	A	9	3418.4	83.5%	112.5%	3405.7	83.2%	112.1%
M4	A	10	3418.7	83.5%	112.5%	3406.8	83.2%	112.2%
M4	A	11	3406.7	83.2%	112.2%	3404.8	83.1%	112.1%
M4	A	12	3412.2	83.3%	111.9%	3403.4	83.1%	111.6%
M4	A	13	3402.2	83.1%	112.0%	3393.6	82.9%	111.7%
M4	A	14	3422.4	83.6%	112.7%	3415.1	83.4%	112.4%
M4	A	15	3420.1	83.5%	113.0%	3422.7	83.6%	113.1%
M4	A	16	3390.9	82.8%	113.3%	3386.8	82.7%	113.2%
M4	B	1	3418.1	83.5%	115.5%	3416.1	83.4%	115.4%
M4	B	2	3415.8	83.4%	115.0%	3412.6	83.3%	114.9%
M4	B	3	3390.6	82.8%	113.3%	3397.5	83.0%	113.5%
M4	B	4	3393.1	82.9%	113.4%	3395.6	82.9%	113.5%
M4	B	5	3401.2	83.1%	113.2%	3398.8	83.0%	113.2%
M4	B	6	3405.3	83.2%	113.0%	3408.4	83.2%	113.1%
M4	B	7	3417.2	83.4%	112.9%	3419.6	83.5%	113.0%
M4	B	8	3403.9	83.1%	112.5%	3408.6	83.2%	112.6%
M4	B	9	3417.1	83.4%	112.5%	3419.6	83.5%	112.6%
M4	B	10	3424.7	83.6%	112.7%	3421.6	83.6%	112.6%
M4	B	11	3418.4	83.5%	112.5%	3416.9	83.4%	112.5%
M4	B	12	3409.8	83.3%	111.8%	3417.8	83.5%	112.1%
M4	B	13	3401.2	83.1%	112.0%	3404.2	83.1%	112.1%
M4	B	14	3422.8	83.6%	112.7%	3420.2	83.5%	112.6%
M4	B	15	3415.6	83.4%	112.9%	3410.3	83.3%	112.7%
M4	B	16	3386.2	82.7%	113.2%	3389.7	82.8%	113.3%

Table 6: M5 gain transition from RC-01 Part 4 Cold plateau

Band	HAM	Detector	High to Low Transition			Low to High Transition		
			dn at transistion	% of 4095	% of dn_{MAX}	dn at transistion	% of 4095	% of dn_{MAX}
M5	A	1	3412.4	83.3%	113.0%	3405.6	83.2%	112.8%
M5	A	2	3399.0	83.0%	113.2%	3391.6	82.8%	112.9%
M5	A	3	3392.3	82.8%	112.4%	3396.9	83.0%	112.5%
M5	A	4	3370.8	82.3%	111.7%	3378.0	82.5%	111.9%
M5	A	5	3388.5	82.7%	111.7%	3387.5	82.7%	111.6%
M5	A	6	3395.5	82.9%	111.9%	3392.9	82.9%	111.8%
M5	A	7	3403.6	83.1%	112.2%	3393.2	82.9%	111.8%
M5	A	8	3393.0	82.9%	111.3%	3377.7	82.5%	110.7%
M5	A	9	3400.6	83.0%	111.5%	3406.8	83.2%	111.7%
M5	A	10	3410.2	83.3%	111.8%	3402.3	83.1%	111.6%
M5	A	11	3415.2	83.4%	112.0%	3409.9	83.3%	111.8%
M5	A	12	3398.8	83.0%	111.4%	3397.4	83.0%	111.4%
M5	A	13	3400.6	83.0%	111.5%	3397.8	83.0%	111.4%
M5	A	14	3405.0	83.2%	112.2%	3396.4	82.9%	111.9%
M5	A	15	3396.2	82.9%	111.9%	3400.9	83.0%	112.1%
M5	A	16	3391.5	82.8%	112.9%	3383.8	82.6%	112.7%
M5	B	1	3401.5	83.1%	112.7%	3401.8	83.1%	112.7%
M5	B	2	3390.1	82.8%	112.9%	3396.1	82.9%	113.1%
M5	B	3	3404.5	83.1%	112.8%	3384.8	82.7%	112.1%
M5	B	4	3383.4	82.6%	112.1%	3370.5	82.3%	111.6%
M5	B	5	3396.9	83.0%	112.0%	3392.7	82.8%	111.8%
M5	B	6	3385.9	82.7%	111.6%	3384.7	82.7%	111.5%
M5	B	7	3396.6	82.9%	111.9%	3397.7	83.0%	112.0%
M5	B	8	3389.9	82.8%	111.2%	3386.6	82.7%	111.0%
M5	B	9	3409.4	83.3%	111.8%	3400.6	83.0%	111.5%
M5	B	10	3408.3	83.2%	111.8%	3406.1	83.2%	111.7%
M5	B	11	3405.2	83.2%	111.7%	3400.0	83.0%	111.5%
M5	B	12	3387.8	82.7%	111.1%	3402.5	83.1%	111.6%
M5	B	13	3387.1	82.7%	111.1%	3389.0	82.8%	111.1%
M5	B	14	3392.0	82.8%	111.8%	3397.1	83.0%	112.0%
M5	B	15	3405.2	83.2%	112.2%	3396.2	82.9%	111.9%
M5	B	16	3383.6	82.6%	112.6%	3390.3	82.8%	112.9%

Table 7: M7 gain transition from RC-01 Part 4 Cold plateau

Band	HAM	Detector	High to Low Transition			Low to High Transition		
			dn at transistion	% of 4095	% of dn_{MAX}	dn at transistion	% of 4095	% of dn_{MAX}
M7	A	1	3438.9	84.0%	108.4%	3431.0	83.8%	108.1%
M7	A	2	3440.5	84.0%	108.4%	3426.7	83.7%	108.0%
M7	A	3	3418.7	83.5%	108.0%	3414.6	83.4%	107.9%
M7	A	4	3412.7	83.3%	107.5%	3403.1	83.1%	107.1%
M7	A	5	3411.1	83.3%	107.5%	3414.2	83.4%	107.6%
M7	A	6	3409.9	83.3%	106.9%	3396.4	82.9%	106.5%
M7	A	7	3437.0	83.9%	107.7%	3424.3	83.6%	107.3%
M7	A	8	3430.0	83.8%	106.8%	3442.8	84.1%	107.2%
M7	A	9	3444.7	84.1%	107.2%	3443.1	84.1%	107.1%
M7	A	10	3436.6	83.9%	106.9%	3442.7	84.1%	107.1%
M7	A	11	3456.5	84.4%	106.9%	3451.5	84.3%	106.8%
M7	A	12	3398.3	83.0%	105.8%	3392.1	82.8%	105.6%
M7	A	13	3420.5	83.5%	107.0%	3432.3	83.8%	107.4%
M7	A	14	3421.6	83.6%	107.3%	3433.2	83.8%	107.6%
M7	A	15	3426.0	83.7%	108.3%	3401.5	83.1%	107.6%
M7	A	16	3422.7	83.6%	108.4%	3398.4	83.0%	107.6%
M7	B	1	3431.7	83.8%	108.2%	3415.3	83.4%	107.6%
M7	B	2	3436.3	83.9%	108.3%	3410.2	83.3%	107.5%
M7	B	3	3431.2	83.8%	108.4%	3399.0	83.0%	107.4%
M7	B	4	3404.7	83.1%	107.2%	3406.1	83.2%	107.2%
M7	B	5	3405.0	83.1%	107.3%	3398.7	83.0%	107.1%
M7	B	6	3409.0	83.2%	106.9%	3410.9	83.3%	106.9%
M7	B	7	3430.3	83.8%	107.5%	3442.9	84.1%	107.9%
M7	B	8	3434.9	83.9%	107.0%	3429.9	83.8%	106.8%
M7	B	9	3459.2	84.5%	107.6%	3427.6	83.7%	106.6%
M7	B	10	3429.3	83.7%	106.7%	3428.0	83.7%	106.6%
M7	B	11	3449.0	84.2%	106.7%	3441.2	84.0%	106.5%
M7	B	12	3410.0	83.3%	106.2%	3411.9	83.3%	106.3%
M7	B	13	3424.3	83.6%	107.1%	3430.0	83.8%	107.3%
M7	B	14	3436.0	83.9%	107.7%	3418.4	83.5%	107.2%
M7	B	15	3419.2	83.5%	108.1%	3417.8	83.5%	108.1%
M7	B	16	3415.4	83.4%	108.1%	3415.8	83.4%	108.1%

Figure 1: Sample range extracted for the SIS100 view (M1 shown)

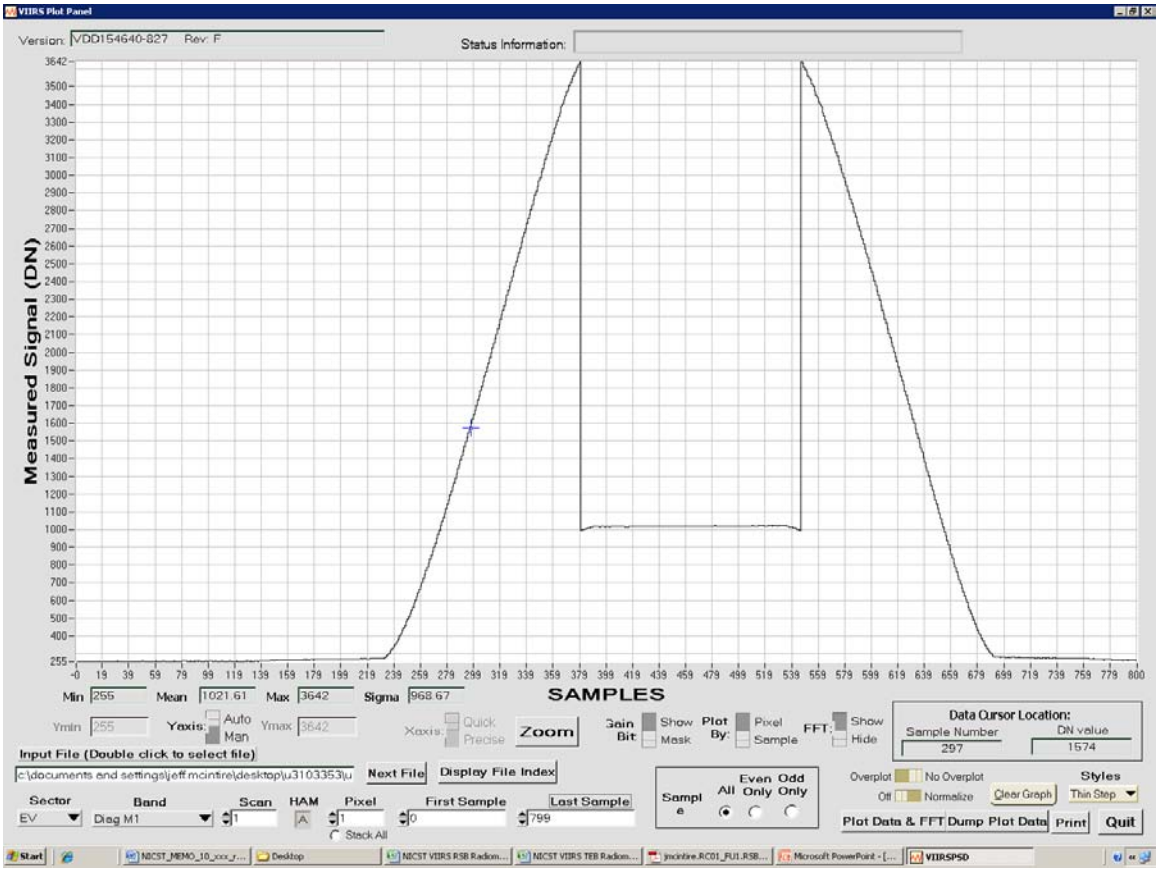

Figure 2: M1 gain transition L ($Wm^{-2}str^{-1}\mu m^{-1}$) from RC-01 Part 4, Ham side A and electronics side A side per detector

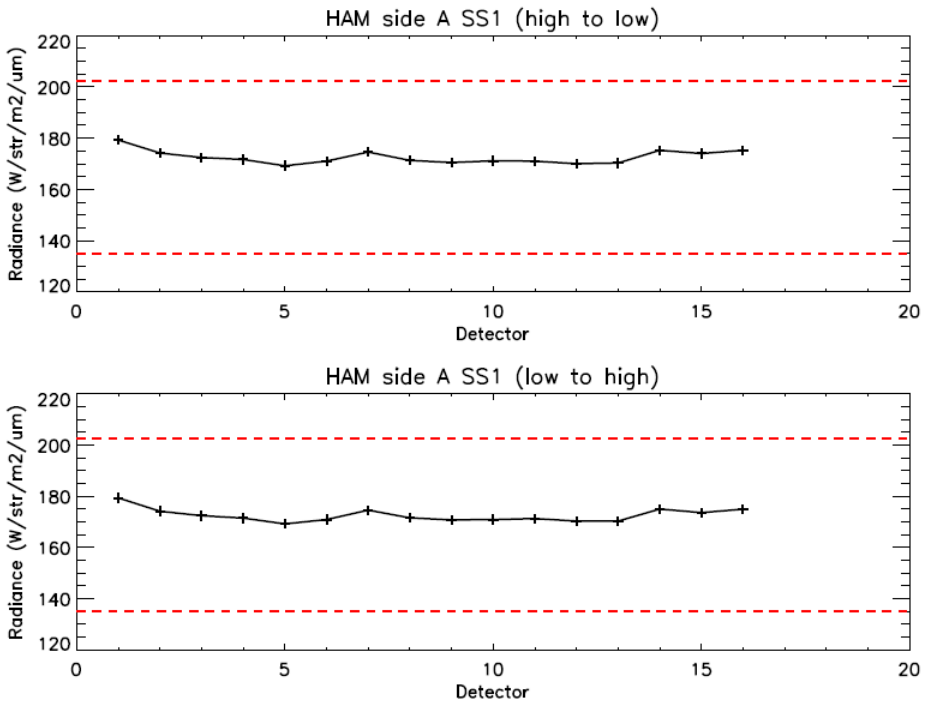

Figure 3: Gain transition dn, standard deviation, and SNR for M1 detector 9 as a function of sample for collect 3

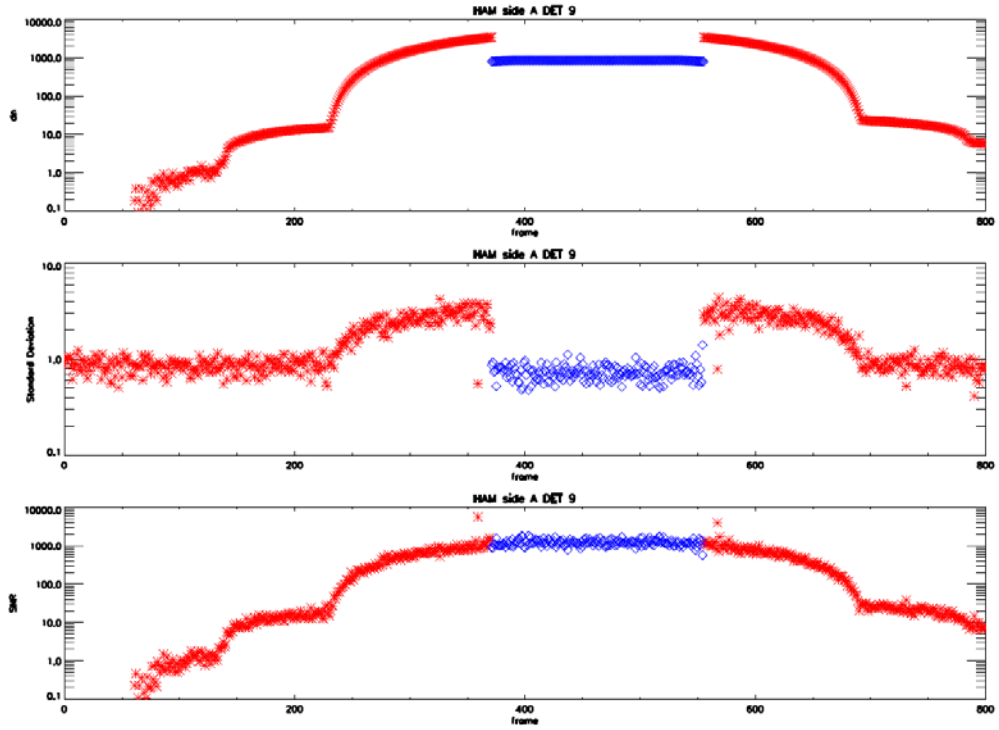

Figure 4: M2 gain transition L ($Wm^{-2}str^{-1}\mu m^{-1}$) from RC-01 Part 4, Ham side A and electronics side A side per detector

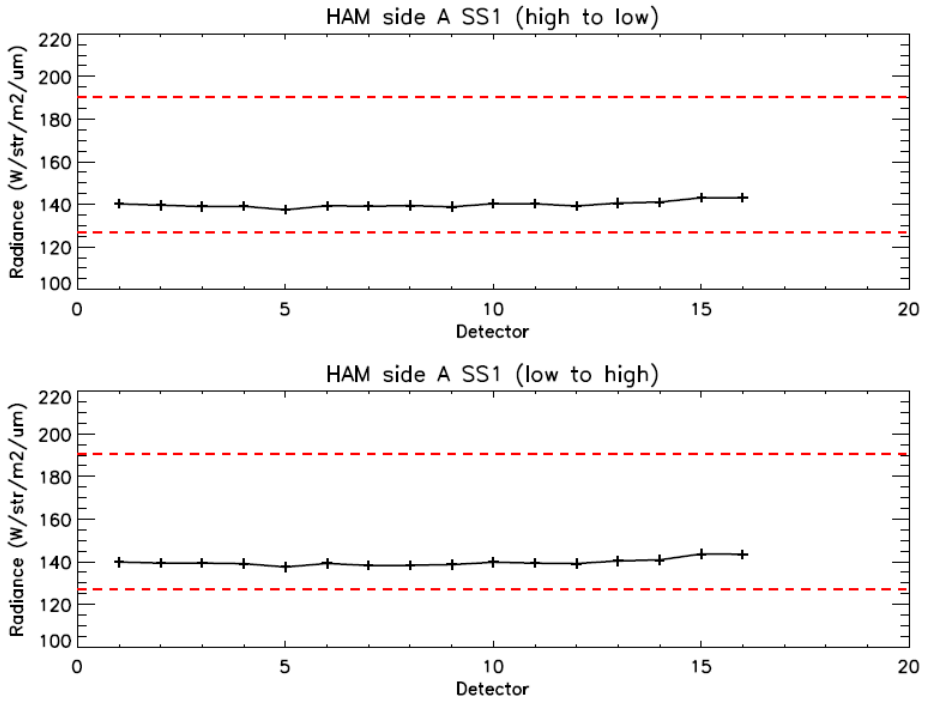

Figure 5: Gain transition dn, standard deviation, and SNR for M2 detector 9 as a function of sample for collect 3

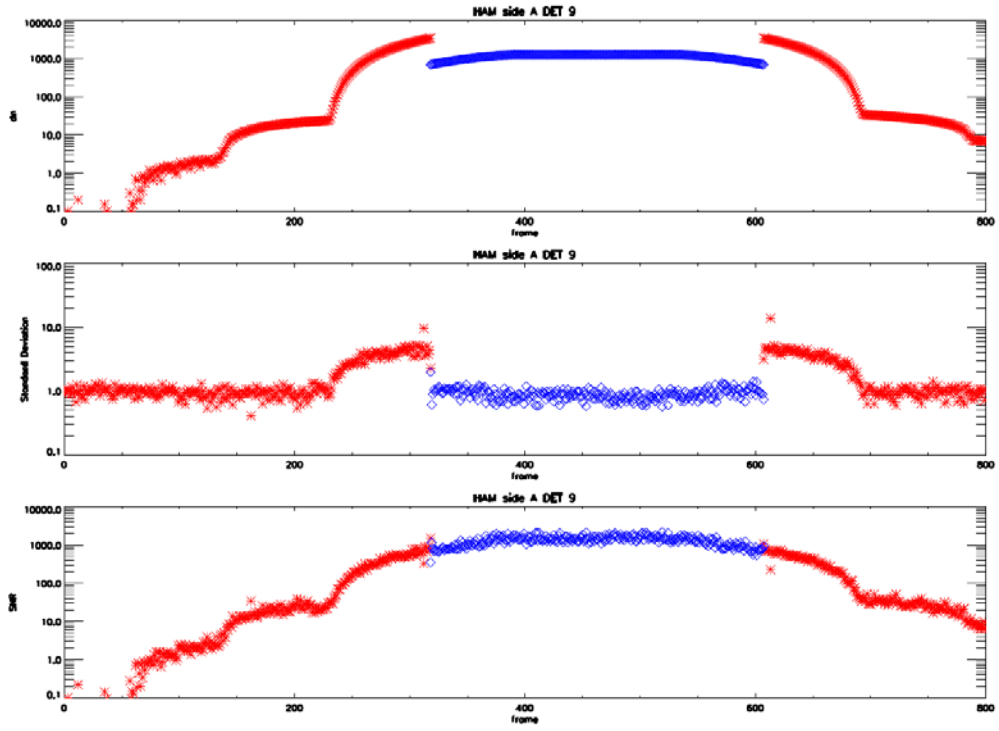

Figure 6: M3 gain transition L ($Wm^{-2}str^{-1}\mu m^{-1}$) from RC-01 Part 4, Ham side A and electronics side A side per detector

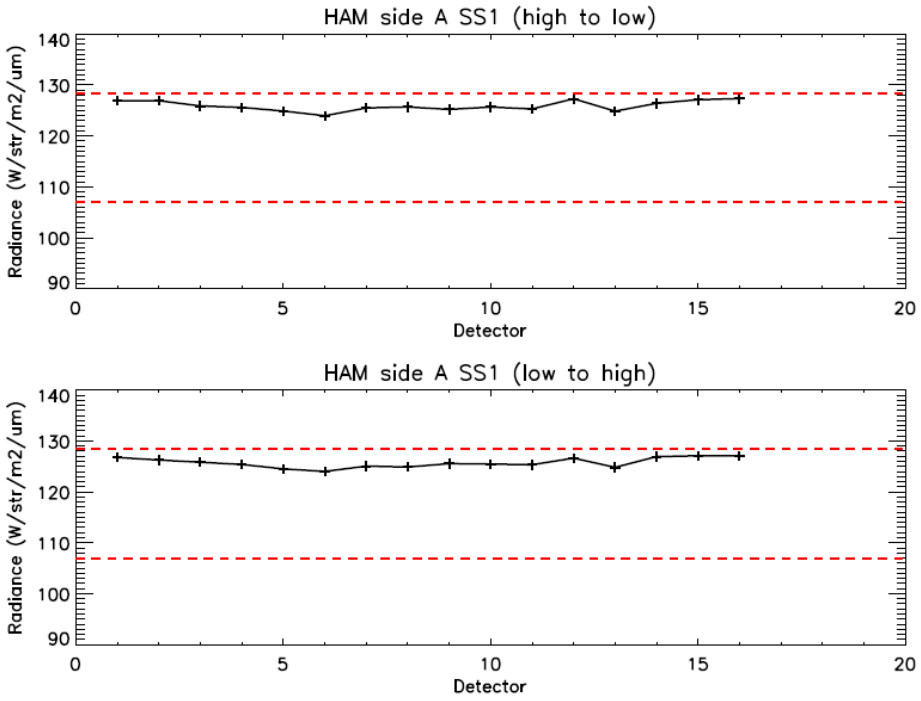

Figure 7: Gain transition dn, standard deviation, and SNR for M3 detector 9 as a function of sample for collect 11

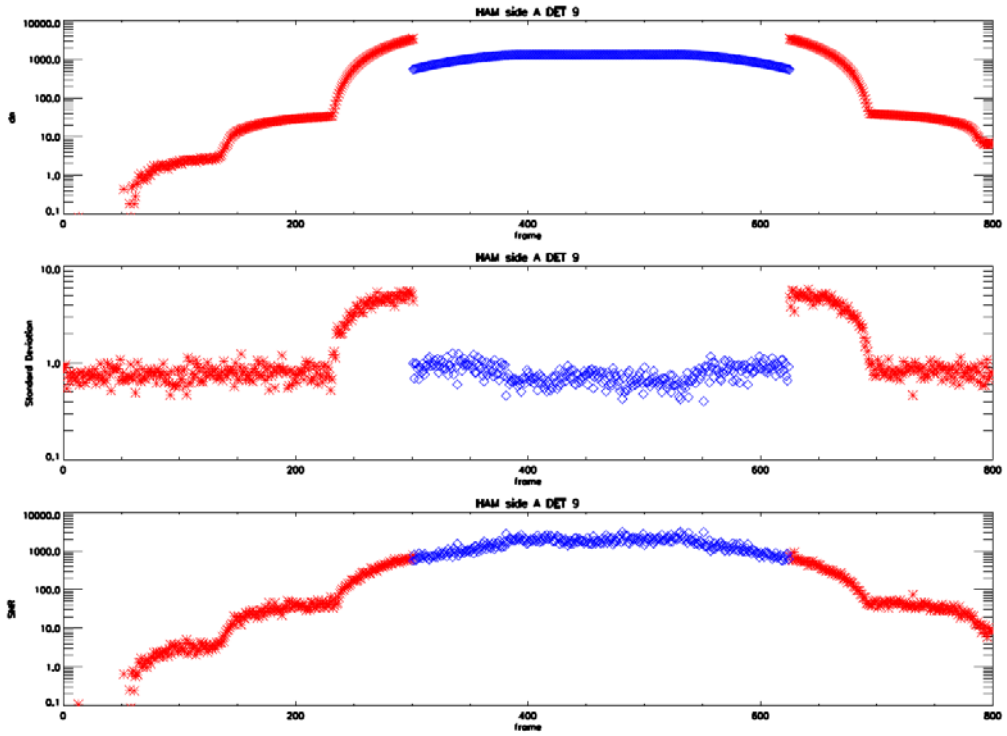

Figure 8: M4 gain transition L ($Wm^{-2}str^{-1}\mu m^{-1}$) from RC-01 Part 4, Ham side A and electronics side A side per detector

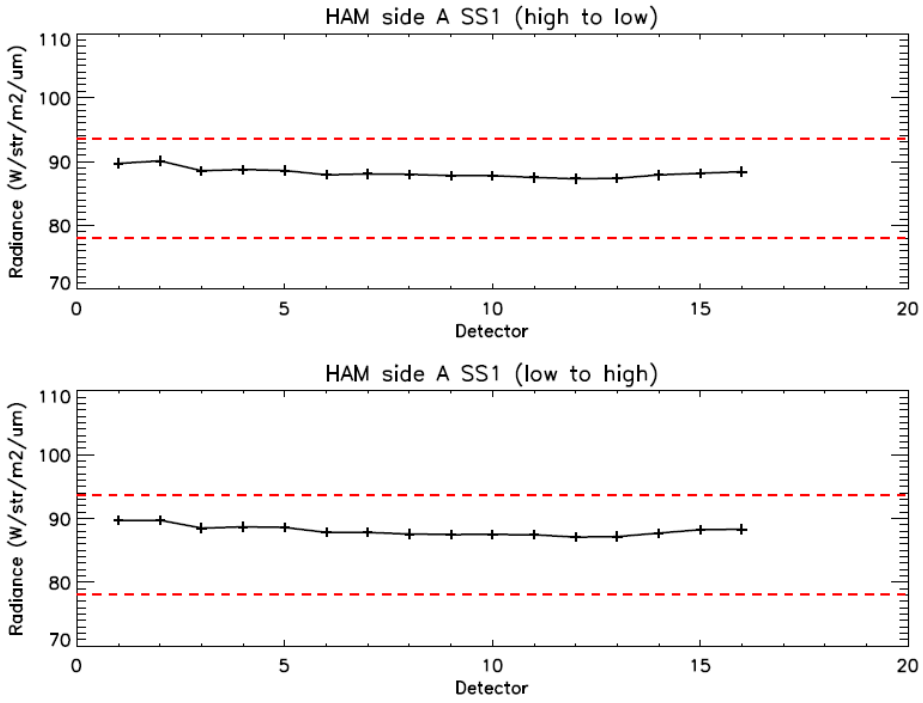

Figure 9: Gain transition dn, standard deviation, and SNR for M4 detector 9 as a function of sample for collect 11

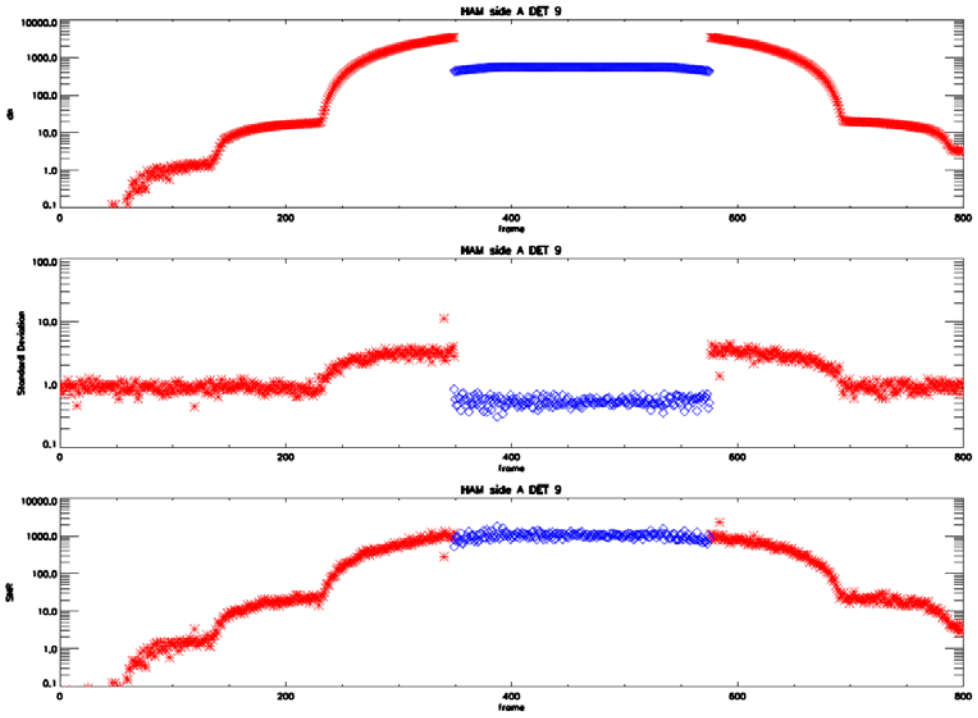

Figure 10: M5 gain transition L ($Wm^{-2}str^{-1}\mu m^{-1}$) from RC-01 Part 4, Ham side A and electronics side A side per detector

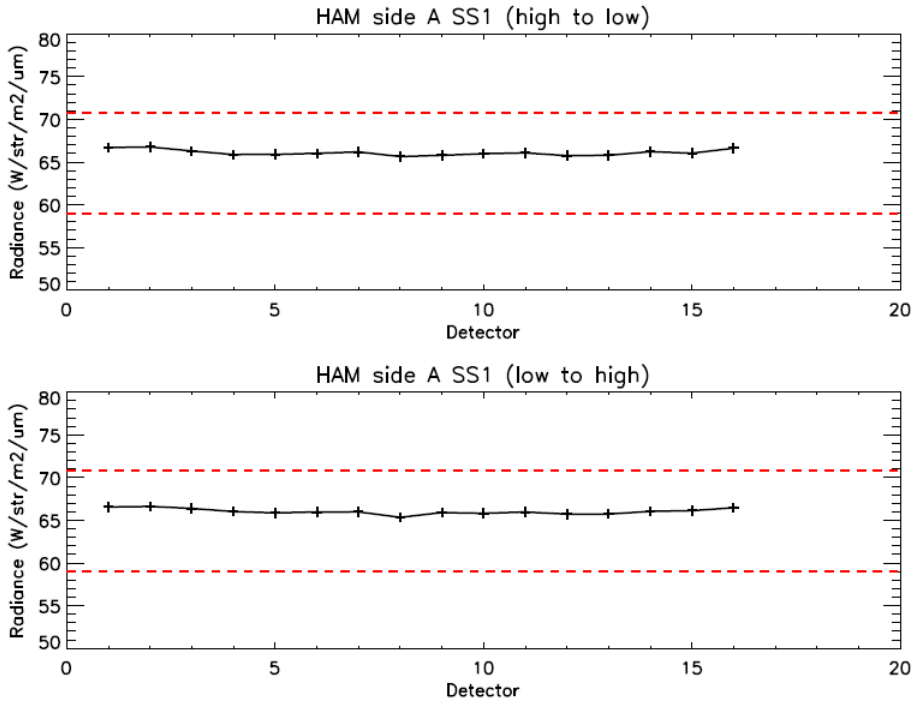

Figure 11: Gain transition dn, standard deviation, and SNR for M5 detector 9 as a function of sample for collect 13

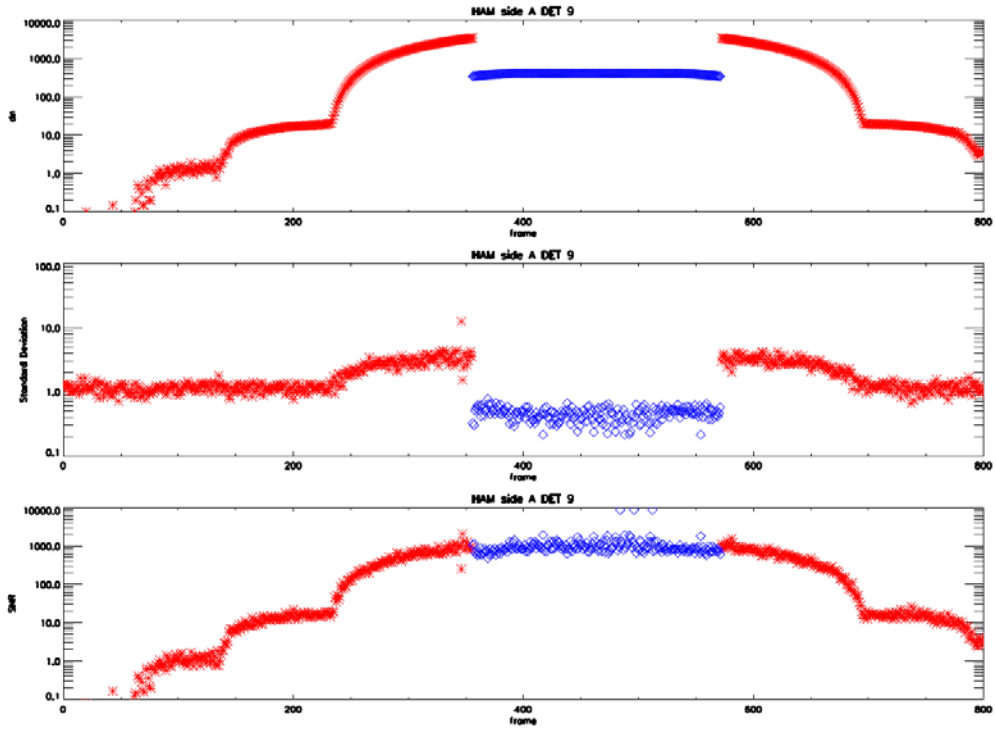

Figure 12: M7 gain transition L ($Wm^{-2}str^{-1}\mu m^{-1}$) from RC-01 Part 4, Ham side A and electronics side A side per detector

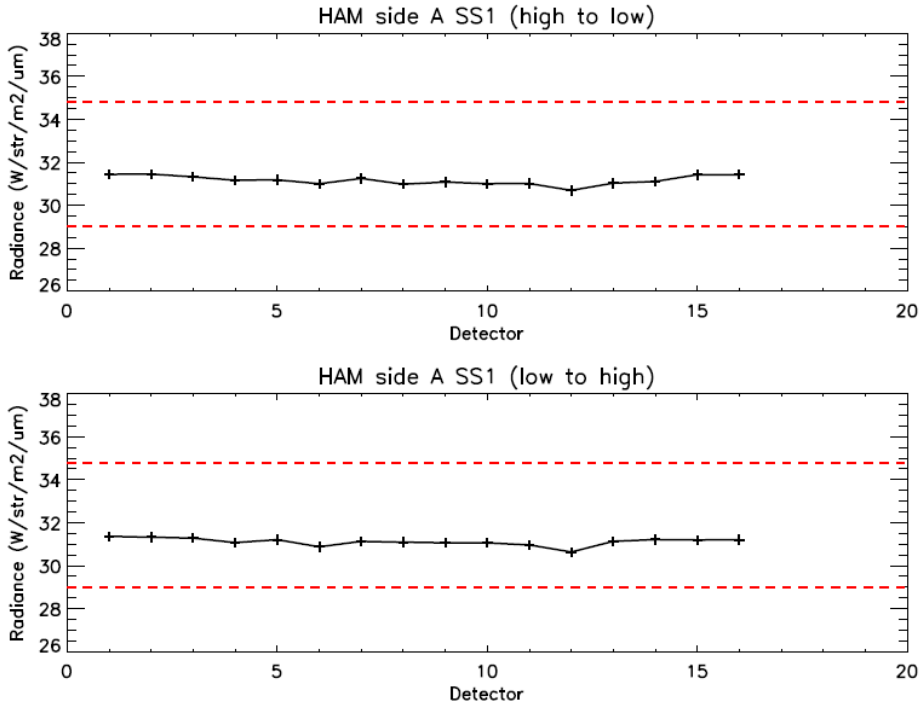

Figure 13: Gain transition dn, standard deviation, and SNR for M7 detector 9 as a function of sample for collect 14